Journal of Materials Chemistry C

Accepted Manuscript

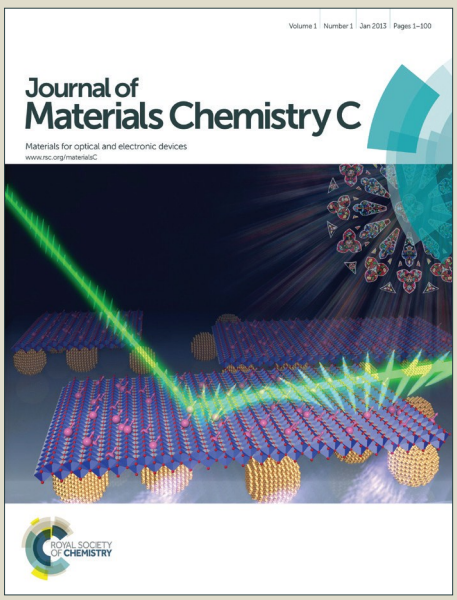

ROYAL SOCIETY OF CHEMISTRY

www.rsc.org/materialsC

Journal Name

ARTICLE

Crystal organometal halide perovskites with promising optoelectronic applications

Received 00th January 20xx,
Accepted 00th January 20xx

DOI: 10.1039/x0xx00000x

www.rsc.org/

Junnian Chen,[a] Shasha Zhou,[a] Shengye Jin,[b] Huiqiao Li[a] and Tianyou Zhai*[a]

Organometal halide perovskites AMX_3 (A=organic cation, M=metal cation, X= halogen anion) have been dominating the photovoltaic fields with an unexpected sharp efficiency enhancement to 20.1% in the past five years. Furthermore, the extraodinary properties of optical absorption, photoluminescence and low non-radiative recombination rate extend their applications into optoelectronic fields beyond photovoltaic devices. This review briefly outlines the state-of-the-art research activities of crystal perovskite AMX_3, describes the fundamental optoelectronic properties, specific morphologies and related synthesis techniques, and summarizes their functions in optoelectronic fields such as solar cells, lasers, light-emitting diodes and photodetectors. Finally, the general challenges and the potential future directions of this exciting research area are highlighted.

1 Introduction

Organometal halide perovskites, described by AMX_3 (A=organic cation, M=metal cation, X=halogen anion) are direct bandgap semiconductors that combine the advantages of crystalline inorganic compounds with those of organic molecules within a molecular-scale composite, possessing attributes of easy process and high carrier mobility.[1] Initial investigations on organometal halide perovskites mainly focus on the synthesis[2,3] and fundamental properties.[4,5,6] In the early 1990s, crystal organometal halide perovskites based field-effect transistors (FETs) and light-emitting diodes (LEDs)[7,8] with good performances were first reported by Mitzi and co-workers, resulting from their outstanding optoelectronic properties.[9,10,11] After Miyasaka et al. fabricated the initial $CH_3NH_3PbX_3$ solar cell in 2009,[12] perovskite material become the prime popular light absorbent. Attributing to the unique properties of strong optical absorption and low non-radiative carrier recombination rates, perovskites AMX_3 renovated the solar cell field in the past five years with the energy conversion efficiency jumped from 3.8% to 20.1%.[13,14,15,16,17] Closely following the rapid development of perovskite solar cells, perovskite film with excellent optoelectronic properties,[18,19] bulk single crystal with low defect density [20] and low dimensional crystal with specific morphologies[21,22,23] evoked new research interests in the applications of LEDs and photodetectors. LED incorporating low-cost organometal halide perovskite with a high luminance of 417 cd m^{-2} has been achieved at room temperature, indicating huge potential for large scale production. [24] Besides, hybrid perovskite photodetector with large detectivity approaching 10^{14} Jones, a linear dynamic range over 100 decibels (dB) and a fast photoresponse with 3-dB bandwidth up to 3 MHz has been demonstrated as well, suggesting great promising in photodetectors. [25] Wavelength-tunable nanowire perovskite $CH_3NH_3PbX_3$ (X=Cl, Br, I) lasing with low threshold (220 nJ cm^{-2}) and high quality factor (Q~3,600) has been observed at room-temperature, making lead halide perovskites ideal material for the development of modern optoelectronic device down to nanoscale.[26] Thus, researches on crystal organometal halide perovskites grow very rapidly in the recent years, as illustrated

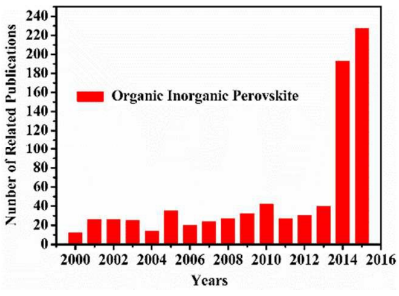

Fig. 1 Publication statistics with respect to perovskites AMX_3. The data was compiled on 23rd 9, 2015 using the ISI database and by applying Topic= (perovskite) and Topic= (organic inorganic)

[a] State Key Laboratory of Material Processing and Die & Mould Technology, School of Materials Science and Engineering, Huazhong University of Science and Technology, Wuhan 430074, P. R. China, *E-mail: zhaity@hust.edu.cn
[b] State Key Laboratory of Molecular Reaction Dynamics, Dalian Institute of Chemical Physics, Chinese Academy of Sciences, Dalian, Liaoning 116023, P. R. China

† Footnotes relating to the title and/or authors should appear here.
Electronic Supplementary Information (ESI) available: [details of any supplementary information available should be included here]. See DOI: 10.1039/x0xx00000x

in Fig. 1. However, recent reviews are mainly concentrated on the photovoltaic applications of organometal halide perovskites,[27,28,29,30] and few review has focused on the research progress of organometal halide perovskites in optoelectronic field as well as the recent development of this kind of material.

In this review, we will provide a summary of the state-of-the-art crystal perovskites material, focusing mainly on the facile synthesis, crystal morphology, unique properties and related optoelectronic applications. We will begin with a historical background of perovskites AMX_3, followed by the description of their fundamental structures, optical and electronic properties. Subsequently, we will introduce crystalline perovskites AMX_3 with specific morphologies and their corresponding synthesis methods. Next, we will exhibit the recent achievements regarding to the potential applications of crystal perovskites AMX_3 in LEDs, lasers, field emitters and photodetectors etc. (Fig. 2). Finally, we will conclude this review with some perspectives and outlook on the development of perovskites material in the near future. Overall, this comprehensive review will provide a summary into the rapid development of crystal perovskites material and their amazing success in optoelectronic field.

2 Fundamental properties of crystal organometal halide perovskites

Organometal halide perovskite AMX_3, isostructural to perovskite $CaTiO_3$ and related oxides, possesses diversity in composition, structure and properties. As can be seen in Fig. 3a, perovskite AMX_3 exhibits a three-dimensional (3-D) network of corner-sharing MX_6 octahedra where a cation occupying the cuboctahedral cavity maintaining the

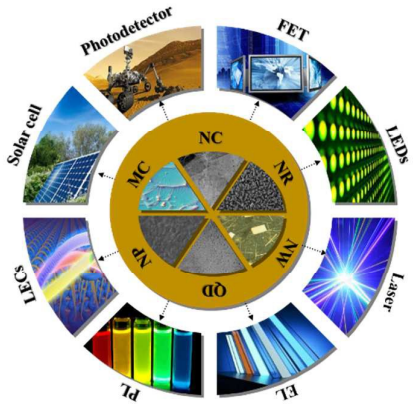

Fig. 2 Schematic diagram showing the potential optoelectronic properties and applications of typical perovskite AMX_3 (acronyms: QD: quantum dots, NW: nanowire, NR: nanorod, NC: nanocrystal, MC: millimeter-scale crystal, NP: nanoparticle, PL: photoluminescence, EL: electroluminescence, LEDs: light-emitting diodes, FET: field-effect transistor and LECs: light-emitting electrochemical cell.)

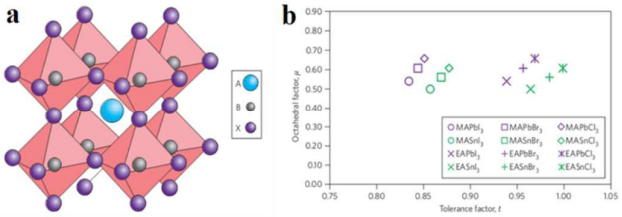

Fig. 3 Perovskite AMX_3 crystal structure and related tolerance and octahedral factors. (a) Crystal structure of cubic perovskite ABX_3. (b) t and μ factors for 12 common organometal halide perovskites. Reproduced from ref. 31 with permission. Copyright 2014 Nature Publishing Group.

electronegativity of the system.[31] The structural probability and crystallographic stability of perovskite AMX_3 can be evaluated via a tolerance factor t and an octahedral factor μ.[32] t is defined as the ratio of the distance A-X to B-X in an idealized solid-sphere model:

$$t = \frac{(R_A + R_X)}{\sqrt{2}(R_B + R_X)} \quad (1)$$

where R_A, R_B and R_X are the ionic radii of the corresponding ions and μ is the ratio of R_B/R_X. The parameters of common perovskites are summarized in Fig. 2b. Generally, for halide perovskites (X = F, Cl, Br, I), $0.81 < t < 1.11$ and $0.44 < \mu < 0.90$ is the confine condition.[33] If t lies in the narrower range of 0.89-1.0, the cubic structure is probably obtained, while lower t values result in less symmetric tetragonal or orthorhombic structures. In addition to the above constraints, perovskites AMX_3 spontaneously undergo transition from the cubic phase at high temperature through one or more tetragonal phases to an orthorhombic phase.[34] The distinguished crystal structure predicts some novel features of halide perovskites, as concisely introduced as follows.

2.1 Optical properties

As the unique attribute of organometal halide perovskites, optical properties of photo-generated charge carriers have been intensively investigated on their strength and resonant behaviour.[35,36] Benefiting from the large exciton binding energy of perovskites $CH_3NH_3PbX_3$ (X = halogen) and their mixed-halide crystals, they show clear excitonic absorption and free-excitonic emission in the visible region at room temperature.[35] Characteristic excitonic absorption peaks in perovskite could be tailored to virtually any wavelength in the visible spectrum through adjusting metal atom (Ge, Sn, and Pb), halogen (Cl, Br, and I) or inorganic sheet thickness.[37] Typical perovskite $CH_3NH_3PbI_3$ exhibits a remarkably steep absorption onset at 825 nm (1.5eV) with a large absorbance coefficient of about 5×10^5 cm^{-1}, which is up to 1 order of magnitude higher than that of GaAs within the visible light range.[38] Further replacing the organic cation of methylammonium (MA) lead iodide with formamidinium (FA), the energy bandgap could be tuned down to 1.48 eV

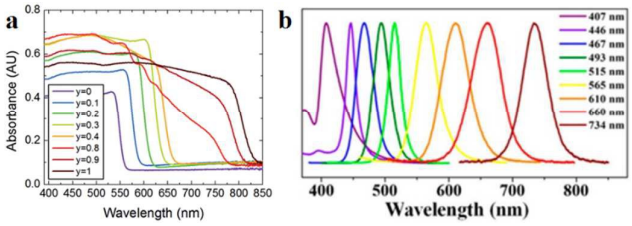

Fig. 4 Absorbance and PL spectra of perovskites. (a) UV-Vis absorption spectra of $FAPbI_yBr_{3-y}$ perovskites. Reproduced from ref. 39 with permission. Copyright 2014 Royal Society of Chemistry. (b) The emission spectra of $CH_3NH_3PbX_3$ QDs. Reproduced from ref. 43 with permission. Copyright 2015 American Chemical Society.

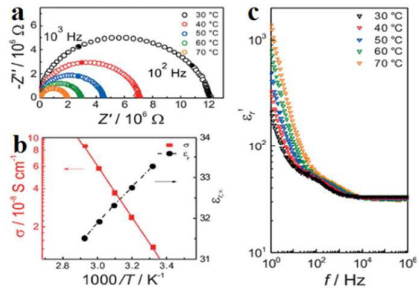

Fig. 5 Electrical properties of $MAPbI_3$. (a) Alternating-current impedance spectra of $MAPbI_3$. (b) Conductivity σ and the bulk relative dielectric constant $\varepsilon_{r,\infty}$ as a function of temperature. (c) Frequency dependent ε'_r (the real part of the complex permittivity). Reproduced from ref. 54 with permission. Copyright 2015 Wiley-VCH.

$(FAPbI_yBr_{3-y})$ (840 nm absorption onset).[39] The onset absorption band of $FAPbI_yBr_{3-y}$ (FA= $HC(NH_2)_2^+$, 0≤y≤1) can be tuned from 838 nm (1.48 eV) to 556 nm wavelength (2.23 eV), and an increase in iodide fraction will gradually red-shift the onset absorption band of $FAPbI_yBr_{3-y}$ (Fig. 4a). The broad and strong light absorbance in the visible wavelength range elects organometal halide perovskite as popular semiconductor in optoelectronic field.

Furthermore, organometal halide perovskites could also emit strong room-temperature photoluminescence (PL) that arises from excitons (radiative recombination of charge carriers) in the inorganic sheets.[40,41] Generally, organometal halide perovskite methylammonium lead halide ($CH_3NH_3PbX_3$) and the partially halide-substituted mixed halides emit strong and broad PL around their band gap energies. Pb perovskites composed of ($CH_3NH_3^+$) or ($HC(NH_2)_2^+$) cation and iodide (anion) emit between 700 and 800 nm while the emission of similar Sn perovskites lie within 850-1000 nm, covering a broad region of near-IR spectrum.[42] Just as optical absorption, the PL of organometal halide perovskites could be affected through modifying organic cations or halide anions. As shown in Fig. 4b, the PL spectra of $CH_3NH_3PbX_3$ QD could be finely tuned from 407 to 734 nm by tailoring the composition of halide anions.[43] PL spectroscopy could reflect some important photo-physical properties such as low exciton binding energies[44,45] and high dielectric constants,[46,47] particularly valuable for the optoelectronic property characterizations of perovskites. The strong and tunable PL indicates that organometal halide perovskites are suitable for a range of light-emitting applications, including lasers, light-emitting devices and optical sensors.

2.2 Electrical properties

In addition to the remarkable optical properties, electrical properties of organometal halide perovskites have caught the attention of scientists as well.[48,49,50] The basic electrical properties such as carrier type, concentration and mobility in perovskites were proved to be greatly influenced by their synthesis methods.[51,52] Through investigating the nature of organometal halide perovskites fabricated from a variety of synthetic approaches, Stoumpos et al. observed that n-type perovskites with the lowest carrier concentration are gained from solution and p-type perovskites can be obtained through solid state reactions.[42] Based on the resistivity, Seebeck and Hall effect investigation, polycrystalline $CH_3NH_3PbI_3$ was demonstrated to show n-type conductivity, carrier concentration of $\sim 10^9$ cm^{-3} and an electron mobility of 66 $cm^2V^{-1}s^{-1}$. While $CH_3NH_3SnI_3$ synthesized by solution processed method shows an electron mobility of 200 $cm^2V^{-1}s^{-1}$,[52] which is much smaller than the 2320 $cm^2V^{-1}s^{-1}$ measured for solid-state reaction in a vacuum-sealed tube.[42] Besides, the high electrical conductivity of $CH_3NH_3Sn_{1-x}Pb_xBr_3$ was found to decrease drastically upon replacement of Sn by Pb, due to the change in the local octahedral environment of $SnBr_6$ and the Sn-Br-Sn bond length.[53]

Yang et al. reported significance of ionic transport in organic lead-iodide based perovskite, and observed higher ionic conductivity than electronic conductivity in $CH_3NH_3PbI_3$.[54] Single distorted semicircle appears in the alternating-current (AC) impedance spectra (Fig. 5a), which is assigned to the pure bulk property ($\varepsilon_{r,\infty}$=34 at 308 ℃) based on the calculated relative dielectric constant.[48] As can be seen in Fig. 5b, $\varepsilon_{r,\infty}$ slightly decreases with the increasing temperature. Bulk conductivity of $CH_3NH_3PbI_3$ increases as temperature goes up with an activation energy of 0.43 eV, in according with previous report.[55] As temperature increases, the real part of the complex permittivity (ε'_r) in high frequencies (>10^4 Hz) slightly decreases (Fig. 5c). In the lower frequency range, ε'_r begins to rapidly rise by an order of magnitude up to 300 at 1Hz and 30 °C and increases with the increased temperature at low frequencies, which resembles the phenomenon observed from $MAPbI_3$-based solar cells.[56] In addition, electrical properties of perovskites have been proved to be affected by the size of the organic cation.

Even in polycrystalline film, organometal halide perovskites with low-cost and low defects density could offer significant advantages over the conventional semiconductors. The extraordinary optical and electronic properties make perovskite a unique semiconductor. Moreover, organometal halide perovskites with chemical tunability of optoelectronic properties could be tailored for various requirements, which have and will continually aroused intensive interests in optoelectronic field.

3 Synthesis of crystal organometal halide perovskites

Synthesis of crystal organometal halide perovskite was first reported by Weber in 1978, who fabricated the cubic perovskite $CH_3NH_3PbX_3$ through mixing the precursor CH_3NH_3 aqueous, concentrated Br_2 aqueous and $Pb(NO_3)_2$ under stir at 100℃.[57] Later, a convenient two-step technique for preparing organometal halide perovskite thin films was developed, during which films of the metal halide MI_2 were deposited onto ash glass or quartz disks using vacuum evaporation or spin-coating and followed by dipping into an organic ammonium iodide solution within a short time at room temperature.[58] With further development of organometal halide perovskites, solution processed [59, 60] and vapor evaporation[61] methods have become the two main effective methods for preparation of perovskites.

3.1 Solution processed methods

Crystal organometal halide perovskites could be easily precipitated from solution through evaporating the precursor metal halide and organic halide by heating or spin-coating. As stated above, heating approach was developed for fabrication of crystal perovskites early in the 1970s.[57] While spin-coating technique is frequently employed in preparation of perovskite film after the birth of perovskite solar cells.[13,25,62,63] Common solvents used for synthesis of perovskites include γ-butyrolactone (GBL), N, N-dimethylformamide (DMF) and dimethylsulphoxide (DMSO). By coating the simply mixed CH_3NH_3I and PbI_2 (in a GBL solution with stoichiometric (1:1) molar ratio) and CH_3NH_3Br and $PbBr_2$ (in a DMF) onto TiO_2 film, $CH_3NH_3PbI_3$ and $CH_3NH_3PbBr_3$ perovskite polycrystalline thin film could be easily obtained at room temperature.[12] Besides, iodide/chloride mixed-halide perovskite $CH_3NH_3PbI_xCl_{3-x}$ film was achieved through spin-coating dissolved MAI and $PbCl_2$ (3:1 molar ratio) or MACl and PbI_2 (1:1 molar ratio) in anhydrous DMF at room temperature.[64] Through introducing toluene drop-casting process after spin-coating precursors in a mixed solvent of GBL and DMSO, Jeon et al. obtained extremely uniform and dense perovskite $MAPb(I_{1-x}Br_x)_3$ layers.[65] The novel solvent-engineering technology provides us new insight in improving the quality of perovskite film. However, the above single-step solution process easily causes uncontrollable precipitation of the perovskites and leads to large morphological variations. Thus two-step solution process emerged in which the lead halide is prepared by spin-coating and then exposed to methylammonium halide for converting into perovskites through spin-coating [66] or dip-coating, [67] gaining better control over the morphology of perovskite films. Mixed-cation perovskite $(MA)_x(FA)_{1-x}PbI_3$ was successfully synthesized via exposure of PbI_2 infiltrated TiO_2 to a solution of FAI and MAI in 2-propanol.[68] Furthermore, employment of solvent annealing technique after two-step solution process was proved to effectively increase the crystallinity and grain size of $CH_3NH_3PbI_3$ film.[66]

Song et al. investigated the formation of perovskite $MAPbI_3$ phase via carrying out systematically study on the structural and optical properties of crystal perovskites fabricated by spin-coating MAI and PbI_2 precursor solutions with different mole fraction, revealing that the obtained $MAPbI_3$ phases were strongly dependent on the reaction temperature and initial compositions.[69] Unexpectedly, chloride as dopant in precursor solution could offer some unexpected improvement in the film morphology and structure, [70, 71] and further work on the mechanism is essential. In conclusion, explore controllable solution processed method for synthesizing perovskite films of uniform, continuous and pinhole-free are still challenging and remains a chief concern.

Along with the development of perovskite polycrystalline films, single crystal perovskites with high quality and purity have also been successfully synthesized. Solution processed method has been proved to be effective ways of growing single crystal perovskites. [9,10] Early in the 1990s, Later, $[NH_2C(I)=NH_2]_3MIs$ crystals were obtained by slowly cooling concentrated hydroidic acid aqueous containing NH_2CN and MI_2 (M=Sn, Pb) in an argon atmosphere.[3] Later, Mitzi et al. successfully synthesized single crystal perovskite $(C_6H_5C_2H_4NH_3)_2PbCl_4$ at room temperature by using a layered solution approach through addition of $C_6H_5C_2H_4NH_2$ onto the top of methanol.[9] Recently, bulk single crystal perovskites of high purity with less grains, boundaries, voids, and surface defects emerged as popular material. [72, 73, 74, 75] Dong et al. synthesized bulk single crystal perovskite $CH_3NH_3PbI_3$ from a supersaturated $CH_3NH_3PbI_3$ solution by using a temperature gradient top-seeded-solution-growth method.[76] The schematic device for growing single crystal $CH_3NH_3PbI_3$ is illustrated in Fig. 6a. The large $MAPbI_3$ single crystals (MSCs) were obtained by the consumption of small MSCs in the bottom, attributing to the small temperature difference between the bottom and top of the solution that induced sufficient convection. Single crystal $CH_3NH_3PbI_3$ exhibits a length and height of 10 and 3.3 mm, respectively (Fig. 6b and c). By employing an antisolvent vapor-assisted crystallization approach, Shi et al. obtained sizable crack-free $CH_3NH_3PbX_3$ single crystals with volumes exceeding 100 cubic millimetres. [77] Fig. 6d displays the schematic synthesis process, where an appropriate antisolvent (dichloromethane) is slowly diffused into a solution containing the perovskite precursors (MAX and PbX_2 in DMF or GBA),

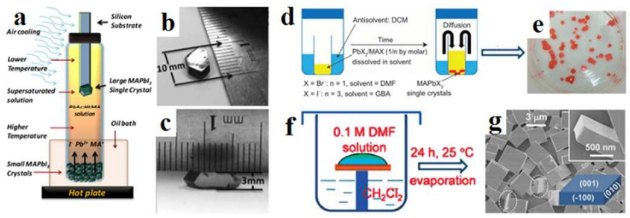

Fig. 6 Synthesis of bulk single crystals perovskites. (a) Schematic diagram for the growth of large $MAPbI_3$ single crystal. Photographs of $MAPbI_3$ single crystal showing its length and height (b) and (c). Reproduced from ref. 76 with permission. Copyright 2015 Science. (d) Illustration of the crystallization process. (e) Photograph of $MAPbBr_3$ single crystals obtained within one week. Reproduced from ref. 77 with permission. Copyright 2015 Science. (f) Fabrication process of $MAPbBr_3$ square microdisk. (g) Low-magnification and high-magnification (top inset) SEM images of $CH_3NH_3PbBr_3$. Reproduced from ref. 78 with permission. Copyright 2015 Wiley.

leading to the growth of sizable $MAPbX_3$ crystals of high quality. Seen from Fig. 6e, the as-grown single crystals $CH_3NH_3PbBr_3$ obtained within one week exhibits length of several hundreds of micrometers. Using a modified solvent/antisolvent (i.e. DMF/DCM) vapor-assisted crystallization approach (Fig. 6f), Liao et al. reported square single-crystalline $CH_3NH_3PbBr_3$ after evaporation of solution for 24 h at room temperature.[78] Fig. 6g shows scanning electron microscope (SEM) image of large amount square $CH_3NH_3PbBr_3$ with smooth outer surfaces and sharp edges. To overcome the time-consuming process for solution growth of single crystal $CH_3NH_3PbX_3$, Saidaminov et al. recently developed an inverse temperature crystallization technique for growing high quality bulk single crystal within minutes.[79] This novel inverse temperature crystallization technique provides us new horizon in synthesizing single crystal $MAPbX_3$ within a short time.

Inspired by the superb optoelectronic properties of bulk perovskites, low dimensional perovskites with specific morphologies have aroused great interests as well.[80,81,82,83] Spin-coating of the filted equimolar mixture of CH_3NH_3I and PbI_2 in γ-butyrolactone solution onto TiO_2 film yielded in situ formed perovskite $CH_3NH_3PbI_3$ nanocrystals with 2-3 nm size.[84] By developing a ligand-assisted reprecipitation (LARP) strategy, Zhang et al. fabricated brightly luminescent and color-tunable colloidal $CH_3NH_3PbX_3$ (X = Br, I, Cl) quantum dots with absolute quantum yield up to 70% at room temperature and low excitation fluencies.[43] Fig. 7a-c schematically illustrate the typical fabrication process of perovskite quantum dots. A mixture of PbX_2, CH_3NH_3X, n-octylamine and oleic acid (Fig. 7b) were dissolved in DMF to form a clear precursor solution (Fig. 7a), and then a fixed amount of the precursor solution was dropped into toluene under vigorous stirring. Followed by a centrifugation at 7000 rpm, colloidal $CH_3NH_3PbX_3$ (X = Br, I, Cl)

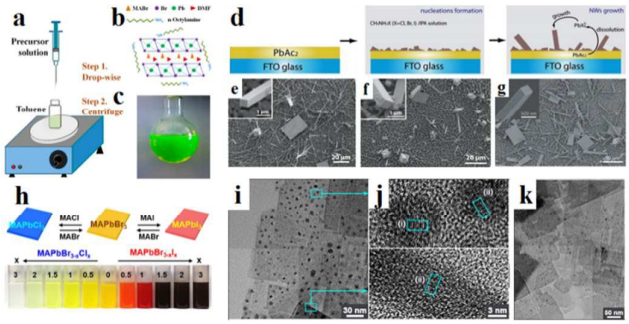

Fig. 7 Synthesis of perovskite $CH_3NH_3PbBr_3$ quantum dots. (a) Schematic illustration of the reaction system and process. (b) Illustration of starting materials. (c) Optical image of colloidal $CH_3NH_3PbBr_3$ solution. Reproduced from ref. 43 with permission. Copyright 2015 American Chemical Society. Synthesis of single crystal perovskite $CH_3NH_3PbX_3$ (X=Cl, Br or I) nanowires. (d) Schematic illustration of the nanowires growth process. SEM images of $CH_3NH_3PbCl_3$ (e), $CH_3NH_3PbBr_3$ (f) and $CH_3NH_3PbI_3$ (g) nanostructures, the insets are the corresponding magnified view. Reproduced from ref. 26 with permission. Copyright 2015 Nature Publishing Group. Synthesis of perovskite $CH_3NH_3PbX_3$ nanocrystals (NCs). (h) Illustration of the reversible anion exchange reaction. (i) HRTEM images of $MAPbBr_3$ NCs. (j) Lattice-resolved images and intensity line profiles for the regions (i) and (ii) of the nanoplates. (k) HRTEM images of $MAPbCl_3$. Reproduced from ref. 86 with permission. Copyright 2015 American Chemical Society.

quantum dots solution is collected (Fig. 7c). Subsequently, Zhuo et al. presented a self-template directed synthesis of porous $CH_3NH_3PbBr_3$ perovskite nanowires with high quality in solution at room temperature, using Pb-containing precursor nanowires as both the sacrificial template and the Pb^{2+} source in the presence of CH_3NH_3Br and HBr.[80] To combine the unique properties of single crystal and low dimension, synthesis of single crystal perovskites with low dimension is already in progress.[85,86] Zhu et al. developed a surface-initiated solution growth strategy that exposed the deposited lead acetate ($PbAc_2$) solid thin film on glass substrate to a high concentration of CH_3NH_3X (X=Cl, Br, or I) solution for fabricating high quality single crystal nanowires.[26] Fig. 7d shows the schematic growth process of single crystal lead halide perovskite nanowires. As shown in Fig. 7e-g, single crystal $CH_3NH_3PbX_3$ nanowires typically have lengths and width up to ~20 μm and 200 nanometers with flat rectangular end facets, respectively. Besides, single crystal plate-type nanocrystals (NCs) $MAPbBr_{3-x}Cl_x$ and $MAPbBr_{3-x}I_x$ NCs were successfully synthesized by halide exchange reaction of $MAPbBr_3$ with MACl and MAI in an isopropyl alcohol solution.[87] The schematic process of the reversible halide exchange reaction is shown in Fig. 7h. The plate-type NCs $MAPbBr_3$ with an average length of 70 nm and a thickness of 15 nm are displayed in Fig. 7i. Seen from Fig. 7j, (200) planes of the lateral side of nanoplates are highlighted which confirms the crystallinity of nanoplates. The dark spots embedded on the nanoplates were inferred as $MAPbBr_3$ nanoparticles. Besides, plate-type NCs $MAPbCl_3$ exchanged from $MAPbBr_3$ exhibits well preserved morphology (Fig. 7k). Besides, Dou et al. synthesized atomically thin two-dimensional organic-inorganic hybrid perovskites $(C_4H_9NH_3)_2PbBr_4$ crystals via a ternary co-solvent solution-phase growth technique.[88] The structure of $(C_4H_9NH_3)_2PbBr_4$ crystal is shown in Fig. 8a, in which six Br atoms surround each Pb atom and the four in-plane Br atoms are shared by two octahedrons, leading to a 2D sheet of $PbBr_4^{2-}$. The edge length of the square crystals $(C_4H_9NH_3)_2PbBr_4$ range from 1 to 10 mm, with an average of 4.2 mm (Fig. 8b). As can be observed in atomic force microscopy (Fig. 8c and d), several monolayer and double-layer sheets show thicknesses

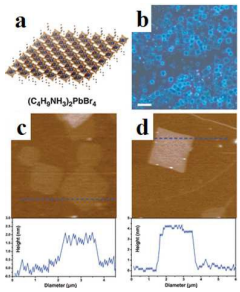

Fig. 8 Synthesis of two dimensional perovskite $(C_4H_9NH_3)_2PbBr_4$ crystals. (a) Schematic of a single layer $(C_4H_9NH_3)_2PbBr_4$ structure. (b) Optical image of the 2D square sheets perovskite. Scale bar is 10 mm. (c) AFM image and height profile of several single layers perovskites. (d) AFM image and height profile of a double layer perovskite. Reproduced from ref. 87 with permission. Copyright 2015 Science.

of 1.6 and 3.4 nm (±0.2 nm). The thickness of the fabricated 2D crystals varied from a few to tens of nanometres. Furthermore, they concluded that the direct solution growth method for fabricating 2D perovskite shows definite advantages over mechanical exfoliation method and solvent exfoliation method, which opens up novel investigation on 2D perovskites and introduces a new family of 2D solution-processed semiconductors for nano-scale optoelectronic devices.

In conclusion, the facile solution process techniques for preparing crystal perovskites $MAPbX_3$ are highly efficient and applicable. However, the disadvantages such as uncontrollable morphology, low repeatability of crystal perovskites and pinhole in perovskites result from solution approaches inhibit the large-scale application. Therefore, developing more efficient and controllable methods for fabricating high quality crystal perovskites $MAPbX_3$ is urgent.

3.2 Vapor evaporation methods

With the development of solution processed methods, vapor evaporation methods have also been employed for producing organometal halide perovskites. Compared to solution approach, vapor evaporation methods tend to produce perovskites with high crystallinity but low yield. By employing in situ X-ray diffraction (XRD)[89] for tracking the phase of perovskites $(CH_3NH_3)Pb(I,Cl)_3$ formed with the vacuum-based coevaporation method, Pistor et al. observed broad miscibility gap in-between different phases. Besides, they found that the composition of the resulting perovskites were strongly depended on the precursor flux ratios, and the synthesized $CH_3NH_3PbI_3$ was conformed to be cubic rather than the usual tetragonal phase that exist at room temperature. Similar to the solution processed method, single-step and sequential step vapor evaporation methods were explored for synthesizing crystal perovskites.

Thermal evaporation has been employed to fabricate perovskite films with better homogeneity and higher crystalline through either co-evaporation[90] or single source evaporation[91] early in the 1990s. The former technique requires the fine balance of the two source evaporation rates which is difficult due to the much higher vapor pressure of the organic component compared to the inorganic counterpart; whereas the latter needs dedicated equipment. Chen et al. synthesized polycrystalline perovskite thin film with full surface coverage, small surface roughness and grain size up to microscale by employing low-temperature vapor-assisted solution process.[92] Furthermore, Liu et al. fabricated compact and uniform flat films of mixed halide perovskite $CH_3NH_3PbI_{3-x}Cl_x$ with low defect density by using a dual-source vapor deposition method.[93]

Chemical vapor deposition (CVD) method has been employed for fabricating low dimensional perovskite crystals as well. Via a two-step chemical vapor deposition (CVD) method, Xiong's group successfully synthesized free-standing $CH_3NH_3PbI_3$ nanowires,[94] $CH_3NH_3PbI_3$ platelets[95] and $CH_3NH_3PbI_{3-a}X_a$ (X=I, Br, Cl) nanoplatelets.[96] Fig. 9a displays the synthesis setup using a vapor-transport system. Xiong et al. obtained single crystal $CH_3NH_3PbI_3$ nanowire with a length up

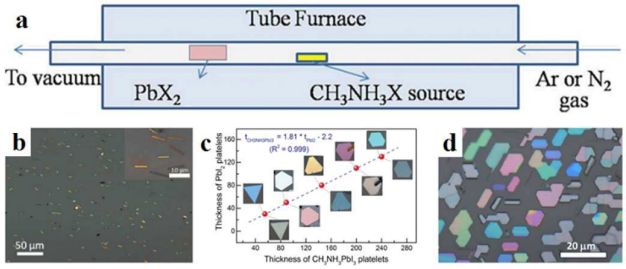

Fig. 9 Illustration of two-step chemical vapor deposition for low dimensional perovskite single crystals. (a) Schematic of the synthesis setup. (b) SEM image of $CH_3NH_3PbI_3$ nanowires. Insets is their corresponding SAED patterns. Reproduced from ref. 93 with permission. Copyright 2015 American Chemical Society. (c) Thickness of PbI_2 platelets before and after being converted to $CH_3NH_3PbI_3$. Reproduced from ref. 94 with permission. Copyright 2014 American Chemical Society. (d) Optical image of $CH_3NH_3PbI_{3-a}Cl_a$ nanoplatelets. Reproduced from ref. 95 with permission. Copyright 2014 Wiely.

to 20 μm and width of ca. 500 nm (Fig. 9b) by converting PbI_2 nanowires (which were first synthesized on silicon oxide substrates by CVD method at 380°C) through a gas-solid hetero-phase reaction.[94] Using freshly cleaved muscovite mica substrate with a similar CVD method, they converted PbI_2 platelets into $CH_3NH_3PbI_3$ platelets through intercalation of CH_3NH_3I.[95] As shown in Fig. 9c, the thickness of PbI_2 and $CH_3NH_3PbI_3$ platelets (before and after conversion) correlates to each other by a factor of 1.81 and the geometries of $CH_3NH_3PbI_3$ preserves that of PbI_2. By adjusting the conversion temperature and pressure of PbX_2 platelets, they further synthesized $CH_3NH_3PbI_{3-a}X_a$ nanoplatelets.[96] The morphologies of lead halides are maintained after its conversion into perovskites exhibiting triangular or hexagonal platelets with nanoscale thickness (10-300 nm) and edge length of several to tens of micrometres (Fig. 9d and e).

4. Optoelectronic applications of crystal organometal halide perovskites

The dramatic rise of organometal halide perovskites in solar cells has aroused the interests of scientists across all over the world. The strong and intense PL, low non-radiative recombination rates and long carrier lifetime in pure and mixed-composition perovskites extend their applications into optoelectronic field such as light-emitting diodes (LEDs), laser and photodetectors. Organometal halide perovskites thus evoke new research interests in optoelectronic filed. Next, we will discuss the up to date research progress of perovskites in optoelectronic field.

4.1 Perovskite solar cells

Recently, many reports have focused on the organometal halide perovskite solar cells, describing the basic fundamentals of perovskite materials, device structure and fabrication for better understanding of the high-efficiency perovskite solar

cells.[31, 97, 98, 99] Integrating high efficiency, ease process procedures and low cost together, perovskite solar

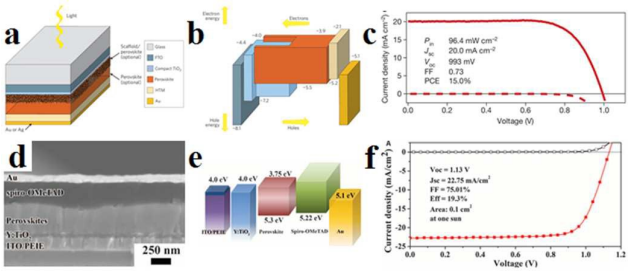

Fig. 10 Mesoporous $CH_3NH_3PbI_3$ based perovskite solar cell. (a) Mesoporous perovskite solar cell configuration. (b) Vacuum energy levels for corresponding component in solar cell. Reproduced from ref. 31 with permission. Copyright 2014 Nature Publishing Group. (c) J-V characteristics for a best-performing cell. Reproduced from ref. 67 with permission. Copyright 2013 Nature Publishing Group. Planar $CH_3NH_3PbI_{3-x}Cl_x$ based perovskite solar cell. (d) SEM image of the planar perovskite solar cell. (e) Vacuum energy levels of each functional layer in the device. (f) J-V characteristics for the champion cell. Reproduced from ref. 15 with permission. Copyright 2014 Science.

cells have shown great promise for practical applications. Solar cells employing perovskite as absorbents originated from the field of dye-sensitized solar cells (DSSCs).[100] Organometal halide perovskite was first used as sensitizer in liquid DSSC in 2009, showing an efficiency of only 3.8% based on perovskite $CH_3NH_3PbI_3$.[101] Because perovskite easily dissolve and degrade in organic liquid electrolyte, initial perovskite solar cells were unstable. Real breakthrough were achieved following the exploitation of solid state hole transport material in perovskite solar cells. By replacing liquid electrolyte with solid hole conductor spiro-MeOTAD (2, 2', 7, 7'-tetrakis-x-2', 7, 7'-tetrakis-9, 9'-spirobifluorene)[102] and poly-triarylamine[63] in perovskite solar cells, enhanced power conversion efficiencies (PCE) of 9.7% and 12% were gained. Subsequently, Burschka et al. developed a sequential deposition method for the formation of perovskite within the porous metal oxide film, and achieved a higher efficiency of approximately 15% with increased reproducibility.[67] Fig. 10a depicts the schematic mesoporous perovskite solar cell configuration.[31] And the vacuum energy levels for corresponding component in solar cell are illustrated in Fig. 10b, which indicates the efficient separation of electrons and holes. Seen from Fig. 10c, the best-performing solar cell yields a high efficiency of 15%, with the open-circuit voltage (V_{OC}), short-circuit current (J_{SC}) and fill factor (*FF*) of 20.0 mA cm^{-2}, 993 mV and 0.73.[67] Sequential deposition technique for the fabrication of perovskite-sensitized mesoscopic solar cells could achieve both high efficiency and high stability which exhibit remarkable advantages over the previous single deposition technique. Furthermore, combination of delicate interface engineering and metal co-doped spiro-OMeTAD enabled the fabrication of planar perovskite solar cells in air and from solution at low temperatures, yielding a robust PCE of 19.3%.[15] Typical SEM image of the solar cell structure is shown in Fig. 10d. Differing from common perovskite solar cell, ITO (Indium Tin Oxide) modified with poly-ethyleneimine ethoxylated (PEIE) was used to reduce the work function. Besides, Yttrium-doped TiO_2 (Y-TiO_2) was used as the electron transport layer (ETL) to enhance electron extraction and transport. As can be observed in Fig. 10e, the favourable energy match between the CBM (conduction band minimum) of the Y-TiO_2 and the HOMO (highest occupied molecular orbital) of spiro-OMeTAD with the CBM and VBM (valence band maximum) of the perovskites allows for efficient extraction of photogenerated carriers within perovskites. Seen from Fig. 10f, the optimized perovskite solar cell gains a PCE of 19.3% under AM 1.5 illumination without antireflective coating, with the V_{OC}, J_{SC} and *FF* of 1.13 V, 22.75 mA cm^{-2} and 0.75, respectively. Very recently, by replacing CH_3NH_3 of $CH_3NH_3PbI_3$ by FA analogue through an intramolecular exchange process, a certified record efficiency of 20.1% for perovskite solar cell was proved.[17] Developing novel approaches to increase the perovskite grain size and passivate surface defects are likely to be critical for further advancement of perovskite solar cells.

4.2 Light-emitting electrochemical cells

Light-emitting electrochemical cell (LEC) is a solid-state device that generates light from an electric current. The LEC is composed of an organic semiconductor light active layer sandwiched between two metal electrodes. Pei et al. have developed LEC by addition of an inorganic salt into a mixture of a conjugated luminescent polymer and an ionic conductive polymer in 1995.[103] LECs emerged as a potential alternative to organic light-emitting diodes (OLEDs) owing to the use of air-stable injection layers and/or electrodes and simple device architecture.[104,105] By replacing organic cation $CH_3NH_3^+$ with FA^+, organometal halide perovskite $FAPbBr_3$ nanoparticles (NPs) were successfully synthesized and applied in LECs, exhibiting a stable luminance of around 1-2 cd m^{-2} at low driving currents.[106] Fig. 11a depicts the perovskite NPs based LEC device. Seen from Fig. 11b, both $MAPbBr_3$ and $FAPbBr_3$ exhibit a near band edge emission with a narrow full width at the half-maximum of approximately 19 nm, indicating high crystalline of the prepared NPs. Besides, exchange of MA to FA red-shifts the emission spectrum of perovskite nanoparticles from 532 to 545 nm. Stable luminance of 1-2 cd m^{-2} at low driving currents was achieved for $FAPbBr_3$ materials (Fig. 11c). The report introduces us novel synthesis concept to fabricate $FAPbBr_3$ NPs, and explores new application of organometal halide perovskites in the development of thin-film lighting devices.

4.3 Light-emitting diodes (LEDs)

Light-emitting diodes (LEDs), a kind of solid-state lighting device based on inorganic semiconductors could provide highly efficient and convenient light point sources of different

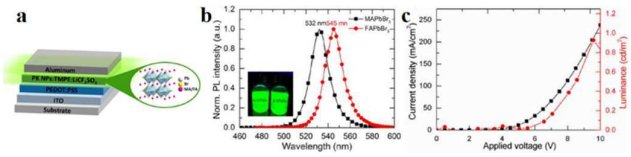

Fig. 11 Hybrid lead halide perovskite nanoparticles based light-emitting electrochemical cells (LECs). (a) Device architecture of the perovskite LECs. (b) PL of $MAPbBr_3$ and $FAPbBr_3$ NPs in THF. Inset is the PL photograph of NPs in THF. (c) Luminance-current density versus applied voltage plot of $FAPbBr_3$ based LECs. Reproduced from ref. 105 with permission. Copyright 2015 American Chemical Society.

colours.[107] The emergence of white LEDs are acquiring an increasing market share in ambient illumination, while challenges such as highly efficient light emission spanning the visible spectrum and exceptional colour quality at low cost still exist.[108] Organometal halide perovskites have the potential to take these challenges, resulting from their extraordinary optical property and compatibility with roll-to-roll solution-processed techniques.[38,109]

Perovskite LEDs were first demonstrated in the 2000s in organometal halide perovskite with organic cations exhibiting layered two-dimensional structures.[8] Recently, organometal halide perovskite aroused new research interest in light-emitting diodes.[110,111,112,113] Tan et al. reported high-brightness light-emitting diodes based on solution-processed organometal halide perovskites $CH_3NH_3PbI_{3-x}Cl_x$, $CH_3NH_3PbBr_3$ and $CH_3NH_3PbI_{3-x}Br_x$, and demonstrated electroluminescence in the near-infrared, green and red by tuning the halide compositions of perovskites at room temperature.[114] The device structure of green $CH_3NH_3PbBr_3$ perovskite light-emitting diode (PrLED) is illustrated in Fig. 12a. $CH_3NH_3PbBr_3$ and $CH_3NH_3PbBr_2I$ PrLEDs emit uniform green and red electroluminescence (Fig. 12b). Seen from Fig. 12c, perovskites with $CH_3NH_3PbBr_3$, $CH_3NH_3PbBr_2I$ (mixed-bromide-iodide perovskite) and $CH_3NH_3PbI_{3-x}Cl_x$ (mixed-chloride-iodide perovskite) compositions emit at green (517 nm) with a luminance of 364 cd m^{-2} and red (630 nm, 754 nm) wavelengths with an infrared radiance of 13.2 W $sr^{-1}m^{-2}$. Furthermore, electroluminescence quantum efficiency of $CH_3NH_3PbBr_3$ PrLED is proved to enhance with the increase of injection current density, which indicates a need for high charge densities to achieve efficient radiative recombination. To avoid the expensive, unstable and low-conductivity properties of fluorenes, Hoye et al. produced fluorene-free PrLEDs by employing spatial atmospheric atomic layer deposition (SAALD) technique that enabled the deposition of ZnO films directly onto $CH_3NH_3PbBr_3$ perovskite, and achieved an improved turn-on voltage and higher luminance than those previously reported results using F8.[115]

With the development of PrLEDs, interface engineering has been proved to be an effective way for improving carrier transport.[116,117] Satisfied emission performance has also been achieved in an inverted $CH_3NH_3PbCl_xBr_yI_{3-x-y}$ based LEDs structure by modifying the conventional PEDOT:PSS hole-injection layer with a perfluorinated polymeric acid.[24] The schematic PrLED structure is displayed in Fig. 12d, in which Buf-HIL is composed of PEDOT:PSS and a perfluorinated polymeric acid (PFI). Fig. 12e shows the green emitting ~~of~~ PrLEDs with high color purity. As can be observed in Fig. 12f, the wide tunability of electroluminescence (EL) spectrum in $CH_3NH_3PbCl_xBr_yI_{3-x-y}$ based PrLEDs is successfully achieved by substitution of Br ions with I ions and Cl ions. Bright flexible perovskite LEDs (PrLEDs) with high spectral purity at room temperature and multicolored PrLEDs by substituting Br^- with I^- and Cl^- ($CH_3NH_3PbCl_xBr_yI_{3-x-y}$) were demonstrated. Much higher luminance, current efficiency (CE) and external quantum efficiency (EQE) (417 cd m^{-2}, 0.577 cd A^{-1}, 0.125%) values than the conventional LED were achieved. Multicolored PrLEDs with

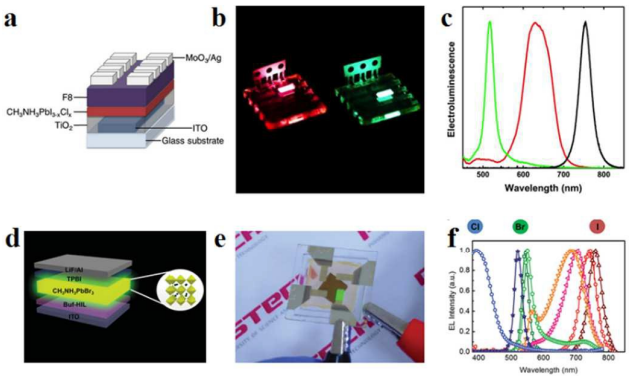

Fig. 12 Bright light-emitting diodes (LEDs) based on perovskites. (a) Device architecture of the $CH_3NH_3PbI_{3-x}Cl_x$ LED. Reproduced from ref. 113 with permission. Copyright 2014 Nature Publishing Group. (b) Photograph of the red and green PeLEDs. (c) EL of perovskite (PrLEDs) with varying halides. Copyright 2015 SPIE. Multicolored perovskite light-emitting diodes (PrLED). (d) PrLED structure based on $CH_3NH_3PbBr_3$. (e) Image of green-emitting PrLEDs. (f) EL of PrLEDs with $CH_3NH_3PbCl_xBryI_{3-x-y}$. Reproduced from ref. 26 with permission. Copyright 2015 Wiley.

high luminance is successfully implemented in the report, which would facilitate the facile large-scale production of efficient flat-panel or flexible displays and solid-state lighting with high color purity. In conclusion, selection of electrode contacts and transport layers with suitable conductivity and band alignment for efficient charge injection is great challenge, and minimizing series resistance from these layers is crucial since perovskite based LEDs operate at high current densities.

Along with the research progress of perovskite film based LEDs, low dimensional perovskites with specific morphologies are gaining increasing attention in LEDs recently. By using a low temperature anion exchange technique, $CH_3NH_3PbBr_3$ nanorod array was successfully converted to $CH_3NH_3PbI_3$ nanorod with preserved morphology, both of which exhibit room temperature EL at room temperature and the application of them in LEDs is further demonstrated.[22]

Organometal halide perovskites based LEDs with high color purity and facile synthesis provide us low-cost and high efficient semiconductor material, which may further accelerate the progress of LEDs. In addition, low dimensional perovskites have demonstrated good performance in LEDs as

well, which provide us new horizon in broaden the investigation of perovskite materials for optoelectronic applications.

4.4 Lasing

Since the first laser implemented a powerful, coherent light source by stimulated emission processes in an optical medium,[118] it has been exploited for wide applications in telecommunications, lighting, displays, medicine and optical physics. Since miniaturization of silicon logic elements has created a bottleneck in inter- and intra-chip communications, the integration of optical interconnects onto silicon chips has become crucial.[119] However, material lattice mismatch and incompatible growth temperatures between high performance III-V semiconductor and silicon have fundamentally restricted monolithic integration of lasers onto silicon substrates,[120] which further inhibit the search for cost-effective, massively scalable and streamlined fabrication of on-chip light sources. Organometal halide perovskites with room temperature solution process and excellent optical properties thus indicates promising application in lasing at room temperature.[121] Biexcitonic lasing has been observed in layered perovskite $(C_6H_{13}NH_3)_2PbI_4$ below 40 K early in the 1990s.[122] Recently, Xing et al. observed an ultra-stable amplified spontaneous emission at strikingly low thresholds of 12±2 μJ cm^{-2} through examining the amplified spontaneous emission (ASE) behavior of solution-processed perovskites $CH_3NH_3PbX_3$ in a cavity-free configuration.[123] Fig. 13a shows room temperature lasing from $CH_3NH_3PbI_3$ film consisted of single crystals, of which optical micrograph of the single crystal is inserted. Wide wavelength tunability of ASE in visible spectral (390-790 nm) through halide substitution of $CH_3NH_3PbI_xCl_yBr_{3-x-y}$ is successfully achieved (Fig. 13b). The emission intensity of perovskite laser increases superlinearly above the threshold fluence of 12±2 μJ m^{-2} (Fig. 13c). Besides, a near invariance of the ASE intensity with a standard deviation of 0.2 % about the mean intensity for ~26 h was observed, revealing excellent optical stability of these perovskite gain media. The above ultra-stable ASE at strikingly low thresholds was supposed to originate from large absorption coefficients, ultralow bulk defect densities and slow Auger recombination in single crystal $CH_3NH_3PbI_3$ film. Furthermore, optically-pumped lasing has also been demonstrated at room temperature in $CH_3NH_3PbI_3$ based polygonal spherical resonators.[121]

Compared to perovskite film, nanostructured perovskite laser with higher performance have been achieved.[23,94] Zhu et al. reported solution processed single crystal lead halide perovskite nanowires $CH_3NH_3PbX_3$ (X=CI, Br, Cl) lasing with low thresholds (220 nJ cm^{-2}), high quality factors (Q~3,600) and near-unity quantum yield.[26] The emission image of a 13.6 μm

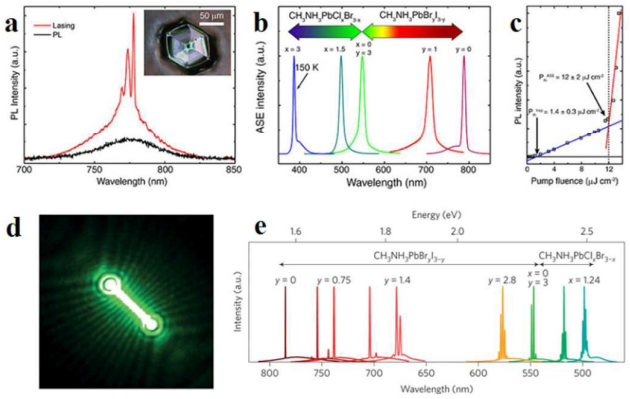

Fig. 13 Perovskites for lasing. (a) $CH_3NH_3PbI_3$ single crystals for lasing at room temperature. Inset is the optical micrograph. (b) Tunable ASE wavelengths from perovskite films. (c) PL intensity of $CH_3NH_3PbI_3$ as a function of pump fluence. Reproduced from ref. 122 with permission. Copyright 2014 Nature Publishing Group. Lead halide perovskite nanowire lasers. (d) Lasing emission image of $CH_3NH_3PbBr_3$. (e) Wide tunability of laser emission at room temperature. Reproduced from ref. 26 with permission. Copyright 2015 Nature Publishing Group.

$CH_3NH_3PbBr_3$ NWs above lasing thresholds is illustrated in Fig. 13d. Widely tunable lasing emission wavelength covering the near-infrared (NIR) to the visible range at room temperature from single crystal nanowire of mixed lead halide perovskites is successfully implemented (Fig. 13e). The extraordinary lasing performance of lead halide perovskite nanowire was due to their long carrier lifetimes and low non-radiative recombination rates. Besides, Xing et al. demonstrated optical-pumped room-temperature visible and near-infrared solid-state nanowire lasers by employing free-standing perovskite nanowires $CH_3NH_3PbI_3$, $CH_3NH_3PbBr_3$ and $CH_3NH_3PbI_xCl_{3-x}$.[94] Furthermore, Zhang et al. reported optically-pumped lasing in polygonal nanocavities based on mixed halide perovskite $CH_3NH_3PbI_{3-a}X_a$ (X = I, Br, Cl) nanoplatelets at room-temperature.[96] The remarkable wavelength tunable whispering-gallery nanolasers can be easily integrated onto conductive platforms with similar threshold of ~40 μJ cm^{-2} and lasing peaks, suggesting the potential of integration onto optoelectronic chips. Liao et al. presented $CH_3NH_3PbBr_3$ whispering-gallery mode WGM microdisk lasers (MDLs) and achieved single mode lasing with a threshold of 3.6±0.5 μJ cm^{-2} and wavelength tunable lasing of perovskite WGM MDLs in the green range from 525 to 557 nm.[78]

Benefiting from large exciton binding energy and low defect density, organometal halide perovskites exhibit superior performance in laser. Single crystal nanowire perovskite lasing with low threshold renovated laser filed, which greatly promoted the development of low dimensional perovskite laser. The superior lasing performance and wide tunability of emission colour across the visible spectrum, combined with the facile solution growth technique make lead halide perovskites excellent material for implementing nanostructured lasers in a wide range of applications, such as nanophotonics, optical computing and chemical/biological sensing.

4.5 Field-effect transistors (FETs)

Field-effect transistors (FET) is consisted of p- or n-type semiconducting channel layers, with the conductivity modulated by applying of a bias voltage to an adjacent insulated conducting gate. Alternative semiconducting materials with mobility comparable to that of amorphous silicon and low-cost process techniques[124] are highly required to enable new opportunities of FETs for display and storage technologies. Organometal halide perovskites perfectly meeting the above demands therefore exhibited great potential in FETs.[125]

Mitzi et al. have carried out intensive work on Tin (II)-based perovskite FETs and demonstrated high mobilities and I_{on}/I_{off} ratio at the beginning of 2000s.[126,127,128] By spin-coating thin

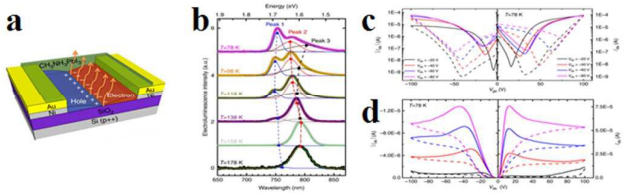

Fig. 14 Lead iodide perovskite field-effect transistor (FET). (a) Schematic of the FET configuration. (b) Low-temperature EL of $CH_3NH_3PbI_3$ FET. (c) Transfer and (d) Output FET characteristics obtained at 78 K. Reproduced from ref. 128 with permission. Copyright 2015 Nature Publishing Group.

film of organometal halide perovskite $(C_6H_5C_2H_4NH_3)_2SnI_4$ to form the conducting channel, they achieved field-effect mobility up to 0.62 $cm^2V^{-1}s^{-1}$and I_{on}/I_{off} ratio above 10^4.[127] Through substituting organic cation in hybrid perovskite for FET, Mitzi et al. achieved a saturation-regime mobility as high as 1.4 $cm^2V^{-1}s^{-1}$ and nearly an order of magnitude lower linear-regime mobility.[127] Afterwards, they made further improvement through melting processed deposition technique, where saturation and linear mobility of 2.6 and 1.7 $cm^2V^{-1}s^{-1}$, I_{on}/I_{off} of 10^6 were achieved.[128]

Chin et al. investigated the intrinsic charge transport parameters of $CH_3NH_3PbI_3$ via fabricating high-quality hybrid perovskite FETs, and found that screening effects associated to ionic transport can be effectively eliminated by lowering the operating temperature of FETs.[129] The schematic of the bottom-gate, bottom contact FET configuration is shown in Fig. 14a. As can be observed in Fig. 14b, EL of $CH_3NH_3PbI_3$ light emitting FET displays three peaks centred at 750 nm (Peak 1), 780 nm (Peak 2) and 800 nm (Peak 3) at the lowest temperature investigated (78 K), with distinct amplitudes and spectral positions at various temperatures. It is observed that Peak 1 and Peak 3 resulting from bound excitons in the low-temperature orthorhombic appear only below 158 K, while Peak 2 related to free excitons in the high temperature and smaller bandgap tetragonal phase[130] dominates the EL spectra at higher temperatures. Reducing the operating temperature turns out to be an effective way to reduce hysteresis effects due to ionic transport/screening, allowing to record transport characteristics typical of conventional ambipolar semiconductor FETs (Fig. 14c and d). Typical p-type output characteristics are observed at 98 K and lower temperatures (Fig. 14d). Besides, the hysteresis of n- and p-type transfer characteristics of perovskite FET is substantially reduced below 198 and 98 K respectively, in according with the observation of ambipolar output characteristics.

The demonstration of organometal halide perovskite FET paves the way to implement solution-processed perovskites light-emitting devices, and shows remarkable superiority over other conventional semiconductors. Furthermore, Sn and Pb based perovskite light-emitting field-effect transistors provide intrinsic transport parameters to guide the optimization of materials and solar cells, and will promote the development of novel electro-optic device concepts, such as gated light-emitting diodes and lasers operating at room temperature.

4.6 Photodetector

Photodetector that convert incident light into electrical signal is critical for a variety of industrial and scientific applications such as optical communications, environmental monitoring, day- and night-time surveillance and chemical/biological sensing.[131,132] To achieve high performance photodetectors, exploit semiconductor materials with high absorption extinction coefficient and large charge carrier mobility for ensuring sufficient light absorption and high photocurrent is emergent. Similar to GaAs, $CH_3NH_3PbI_3$ possesses strong light absorption and activity of long-lived photocarriers for high-yield quantum conversion exhibited high photoconductive gain in photodetectors.[133,134,135]

Xie et al. reported the first solution-processed organolead halide perovskite photodetector based on $MAPbI_3$ film and flexible substrates, and gained broad photoresponse range from 780 to 310 nm.[136] The photoresponsivity and EQE of the $MAPbI_3$ film-based flexible photodetectors achieved 3.49 A W^{-1} and 1.19 $\times10^3$ % at 365 nm, revealing high sensitivity, fast response speed and excellent stability. Subsequently, Dou et al. reported solution-processed photodetector based on hybrid perovskite $CH_3NH_3PbI_{3-x}Cl_x$ using an inverted device structure.[25] The inverted device structure of the hybrid perovskite photodetector is displayed in Fig. 15a. Three types of devices were fabricated: PD1 without buffer, PD2 and PD3 with BCP (2,9-dimethyl-4,7-diphenyl-1,10-phenanthroline) and PFN (poly[(9,9-bis(3'-(N,N-dimethylamino)propyl)-2,7-fluorene)-alt-2,7-(9,9-dioctylfluorene)) as cathode buffer layers, respectively. Seen from Fig. 15b, PD3 shows a significantly reduced J_d (dark current), a good rectification ratio of $\sim10^5$ (±1V) and a very high detectivity of 8×10^{13} Jones at -100 mV. The marked increase in forward bias injection of PD3 was attributed to a formation of dipole layer at the PCBM and Al interface which provides an extra electric field to prevent the

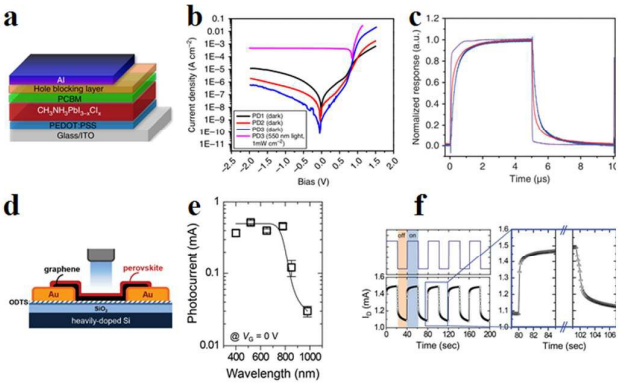

Fig. 15 Solution-processed hybrid perovskite photodetectors. (a) Device structure of the hybrid perovskite photodetector. (b) Current density-voltage curves of photodetectors. (c) Transient photocurrent response. A silicon diode is shown for comparison. Reproduced from ref. 25 with permission. Copyright 2014 Nature Publishing Group. Perovskite-graphene hybrid photodetector. (d) Schematic diagram of the device. (e) Photocurrents of the hybrid photodetector as a function of the illumination wavelength. (f) Transient photocurrent response of the hybrid photodetector. Reproduced from ref. 144 with permission. Copyright 2015 Wiely.

hole injection while enhance electron injection. The transient response results for the device with 0.01 cm^2 area show a rise time of 180 ns and a decay time of 160 ns, while the rise time and decay time for a device with 0.1 cm^2 area are both ~600 ns (Fig. 15c). Besides, the quantum efficiency remains almost constant under different incident power density, which suggests that perovskite photodetector is well suited for detecting a wide range of incident powers. Subsequently, novel device structures for perovskite photodetectors emerged as popular approach and turned out to be effective.[137,138]

Following the development of novel device structure, implementation of interface engineering emerged as efficient technique for improving the performance of perovskite photodetectors as well.[139,140] Dong et al. reported a high gain solution-processed $CH_3NH_3PbI_3$-based photodetectors with a broadband response ranging from the UV (ultraviolet) to the NIR by introducing 4,4′-bis[(p-trichlorosilylpropyl-phenyl) phenylamino]-biphenyl (TPD-Si_2) as the hole transporting layer in a layered inverted structured photodetector. [141] The photodetector yielded a very high gain of 405±6 and responsivity of 242 A W^{-1} at low bias (-1 V) that originated from hole traps caused by large concentration of Pb^{2+} in the perovskite film surface. Fang et al. reported highly sensitive perovskite photodetector with low noise (16 fA $Hz^{-1/2}$ at -0.1 V) via introducing device interface engineering and perovskite layer morphology improvement. [142] The employment of interfacial electron transport layer (ETL) and hole transport layers (HTL), especially the trap passivation effect of the fullerene layer in device enables its direct measurement of light irradiance down to sub 1 pW cm^{-2}.

With the explosive progress of organometal halide perovskite film based photodetector, low dimensional perovskite of many active sites also aroused great interests in photodetectors.[81, 143] Zhuo et al. demonstrated porous $CH_3NH_3PbBr_3$ nanowires visible-light photodetectors with a photoresponse time of only 0.12s and a decay time of about 0.086s.[80] The high sensitivity and stability of porous

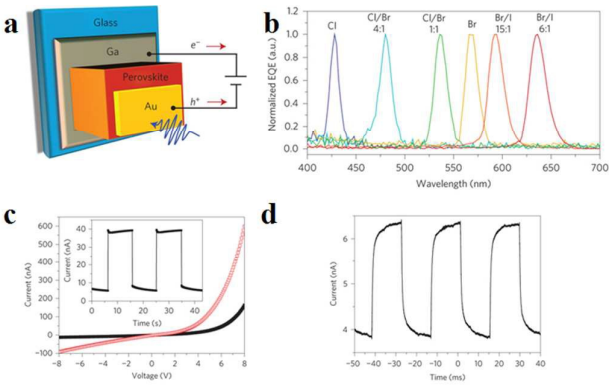

Fig. 16 Narrowband perovskite single-crystal photodetectors. (a) Device structure of the perovskite photodetector. (b) Normalized EQE spectra of the perovskite photodetectors. (c) Dark current and photocurrent of photodetector. Inset: repeated operation of the photodetector. (d) Temporal response. Reproduced from ref. 20 with permission. Copyright 2014 Nature Publishing Group.

$CH_3NH_3PbBr_3$ nanowires were supposed to originate from the unique porous 1D geometry, many active sites and strong light absorption. Jang et al. designed plate-type NCs $MAPbBr_{3-x}Cl_x$ and $MAPbBr_{3-x}I_x$ NCs photodetectors, and observed a strong correlation between the photocurrent and PL decay time.[87] Among the mixed halide perovskites, I-rich composition $MAPbBrI_2$ showed the highest photocurrent and the longest PL decay time, which could be ascribed to its pure tetragonal phase nature. First-principles density-functional theory calculations were employed to further understand the composition-dependent photoconversion efficiency.

To inhibit the rapid recombination of photo-induced electron-hole pairs in perovskite, perovskite hybrid photodetectors are gaining increasing attention.[144] Lee et al. developed methylammonium lead halide/single-layer graphene hybridized photodetectors with photoresponse and quantum efficiency of 180 A W^{-1} and 5×10^4 % at a relatively high illumination power of 1 μW.[145] Fig. 15d illustrates the structure of $CH_3NH_3PbI_3$ perovskite/graphene hybrid photodetector fabricated on a SiO_2/Si substrate. Seen from Fig. 15e, a milliampere photocurrent was generated under illumination at wavelengths shorter than 800 nm, which is much higher than the pristine graphene photodetector. The broad spectral photo-responsivity between 800 and 400 nm was attributed to an increase in the optical absorption and photogating mechanisms of the hybrid photodetector. Based on the temporal response of the photocurrent, the rise and fall times of perovskite-graphene hybrid photodetector were calculated to be 87 and 540 ms, indicating good on-off switching behaviour (Fig. 15f). Besides, the on-off switching behavior could maintain for multiple cycles, suggesting the robustness and reproducibility of the perovskite/graphene hybrid photodetectors. Afterwards, Spina et al. designed $MAPbI_3$ nanowire/graphene hybrid photodetector, and gained

a photoresponsivity as high as 2.6×10^6 A W^{-1} that was four orders of magnitude higher than the above hybrid perovskite photodetector.[146] The high device performance of hybrid photodetector was mainly attributed to the nanowire perovskite morphology. The successful demonstration of graphene/perovskite hybrids photodetectors would encourage scientists to further investigate perovskite hybrid photodetectors.

Besides, there is a breakthrough in intrinsically narrowband photodetection with a widely tunable response range employing hybrid perovskite $MAPbBr_{3-x}Cl_x$ and $MAPbI_{3-x}Br_x$ single-crystal-based photodetectors recently.[20] Fig. 16a illustrates the structure of single crystal perovskite photodetector. As seen in Fig. 16b, single crystals perovskites exhibit a single narrow peak close to the absorption edge of each kind of single crystal of different halide compositions, of which full-width at half-maximum are less than 20 nm, enabling narrowband photodetection. The narrowband photodetection was summarized to result from the surface-charge recombination-induced suppression of charge collection for short-wavelength excitation through a comparison of the device modelling results and EQE spectra. Furthermore, the response spectrum of photodetector can be continuously modulated in the visible range from blue to red by adjusting the halide composition of solution processed single crystal. The 1.2-mm-thick $MAPbBr_3$ single-crystal photodetector yields a stable photocurrent and dark current output (Fig. 16c). Fig. 16d records the temporal response with −4V bias under 570 nm LED illumination with light intensities of 6μW cm^{-2} and a modulation frequency of 150 Hz. In addition, the EQE spectra remained almost constant after prolonged exposure to air for both single-halide and mixed-halide perovskite single crystals, revealing better stability compared to their polycrystalline thin-film counterparts. This report provides us novel design paradigm for narrowband photodetector with low-cost and facile fabrication in broader applications where background noise emission needs to be suppressed.

Unlike traditional inorganic semiconductor, the low-temperature solution process enables organometal halide perovskites to deposite on a broader range of substrate materials such as plastics, opening up opportunities to flexible electronic and photonic applications. Besides, the unique optoelectronic properties of perovskites lead to high detectivity and fast response that will greatly promote the research progress of perovskite photodetectors. Furthermore, the successful development of perovskite based hybrid photodetector provides us new horizon in exploring novel device configuration, which is expected to facilitate the development of imaging sensors suitable for low-light photography, UV detectors and smart skin sensors combined with other functionalities.

The remarkable optical properties and photophysical properties of organometal halide perovskites have opened up a multitude of optoelectronic applications beyond solar cells. Satisfied achievements have been obtained in perovskite optoelectronic devices, and the enthusiasm on them will be continually exciting in the future. Along with the successful development of three dimensional perovskites in optoelectronic applications, single crystal and low dimensional perovskites emerged and have demonstrated good performance. We believe that an enormous amount of research interest will be driven to the study of single crystal and low dimensional perovskites in light-emitting applications and optoelectronic devices, guiding new avenue in perovskites research.

5 Conclusions and Outlook

Organometal halide perovskite with extraordinary optoelectronic property has astonished solar cell field with an unprecedented progress, and extended their potential into optoelectronic field. In this focused review, we have summarized the recent research progress of crystalline organometal halide perovskite and their optoelectronic applications. Consider of the achieved progress, organometal halide perovskites are supposed to be excellent candidates for solar cells, LEDs, laser, FETs and photodetectors with good performances. Persistent progress on organometal halide perovskite and their optoelectronic applications will definitely be continuously exciting and highly rewarding. Undoubtedly, there are still many challenges on the roads towards their practical integration into large scale production and application.

Compared to conventional semiconductor-based solar cells, perovskite solar cells hold promise as a low-cost and high efficient alternative.[15] However, almost all of the reported high efficiency perovskite solar cells are achieved on small active area less than 0.1 cm^2, since their energy conversion efficiencies decline quickly with the increased active areas. Therefore, how to fabricate perovskite solar cells with large areas and high quality is a great challenge. Although much intrinsic phenomenon and mechanism has been explored in the recent research efforts, exciting research in searching new hybrid perovskites and revealing the unknown phenomenon and mechanism are still strongly expected.

The development of crystalline organometal halide perovskites and their optoelectronic applications are still in an early stage, there are many unanswered question left in regard to the synthesis, structure, function etc. The highly compatibility of perovskite structure in tailoring their halides, metal and organic cations provides strong support for in-depth investigation of structure-function relationships and further design of new perovskites. For example, mixed halides perovskites $CH_3NH_3PbI_xBr_{1-x}$ or $CH_3NH_3PbI_xCl_{1-x}$ exhibit better stability than that of $CH_3NH_3PbI_3$. Besides, perovskites containing Pb show better stability and performance than that of Sn perovskites. In addition, nanostructured $CH_3NH_3PbX_3$ perovskites show extremely instability under prolonged exposure to the electron beam in TEM and SEM. For low dimensional and single crystal perovskites, the synthesis is a long-term challenge in which crystal nucleation and growth mechanism demands intensive study. Besides, crystallographic

structural and function analysis call for comprehensive study as well. More precise control on morphology, composition and crystallization is required. Among all reported fabrication methods, solution processed method takes obvious advantages in crystal quality and output, much more attention should be paid on the kinetics study. The development of highly efficient and controllable synthesis technique will be helpful for in-depth investigation of the structure-function relationship. In return, understanding the structure-function relationship of perovskites would effectively guide the synthesis of new perovskites.

Although the study on utilization of perovskites in optoelectronic field are growing fast in recent years, some key issues such as the basic concept of p-i-n device structure and attributes of perovskites, especially for the nature of heterojunctions and the origin of long lived charge carriers in perovskites are still ambiguous, which therefore need more scientific attention. Compared to perovskite film contact issue in device, single crystal and low dimensional perovskites with specific morphologies probably undergo a particular interfacial contact mechanism that require extra concern. Employing TiO_2 as compact layer has been proved to be an efficient way to reduce interface barrier potential, indicating applicable approach for modifying the interface contact in perovskite optoelectronic devices. Develop novel compact layer and hole transfer layer with good performances are already under study, suggesting great promising in alleviating or removing the interfacial barrier. Recently, perovskite/graphene hybrid optoelectronic device with inhibited carrier recombination has been successfully implemented, providing us novel horizon in improving performance. In brief, fundamental studies on the photophysical properties, device concept and interfacial charge transfer dynamics should be strengthen for in-depth understanding their extraordinary performances and guiding the design of novel optoelectronic device.

Lastly, to further accelerate the commercial progress of perovskite optoelectronic devices, stability issue of perovskites must be well addressed as soon as possible. Moisture and heat have been proved to be the main two factors causing the degradation of organometal halide perovskites. Besides, perovskites are unstable in the presence of many polar solvents because of their ionic crystals attribute. Essentially, understanding the degradation mechanisms of crystalline perovskite material and searching for efficient approaches to hinder the serious degradation are key issues in the near future. Since stability issue in perovskite solar cells has been improved by porous carbon layer, thus it is natural to extend this strategy to other optoelectronic devices such as photodetectors to improve their stability. Besides, develop proper encapsulation techniques that keep out moisture, oxygen and ultraviolet radiation from perovskites could be effective approach as well.

For optoelectronic devices, low fabrication cost and high device performances are the two critical indexes for practical applications. Combining facile solution processed method with excellent optoelectronic performance, organometal halide perovskites are elected the best candidates among other routine semiconductors. Further study on exploring new technologies for higher reproducibility and stability of perovskites against heat and humidity is highly required, while higher performance is always the long-term challenge for the whole optoelectronic field.

6 Acknowledgements

J. Chen and S. Zhou contributed equally to this work. This work was supported by National Nature Science Foundation of China (21322106 and 51472097), and Ministry of Science and Technology of China (2015CB932600). The authors are indebeted for the kind permission from the corresponding publishers/authors to reproduce their materials, especially figures, used in this article.

Notes and references

1 R. W. G. Wyckoff, *Am. J. Sci.,* 1928, **16**, 349-359.
2 J. Calabrese, N. L. Jones, R. L. Harlow, N. Herron, D. L. Thorn and Y. Wang, *J. Am. Chem. Soc.*, 1991, **113**, 2328-2330.
3 S. M. Wang, D. B. Mitzi, C. A. Field and A. Guloy, *J. Am. Chem. Soc.*, 1995, **117**, 5297-5302.
4 T. Ishihara, J. Takahashi and T. Goto, *Phys. Rev. B*, 1990, **42**, 11099-11107.
5 A. Poglitsch, D. Weber, *J. Chem.Phys.*, 1987, **87**, 6373-6378.
6 I. B. Koutselasy, L. Ducassez and G. C. Papavassiliou, *J. Phys.: Condens. Matter,* 1996, **8**, 1217-1227.
7 D. B. Mitzi, S. Wang, C. A. Feild, C. A. Chess, A. M. Guloy, *Science*, 1995, **267**, 1473-1476.
8 D. B. Mitzi, K. Chondroudis, C. R. Kagan, *IBM J. Res. Dev*., 2001, **45**, 29-45.
9 D. B. Mitzi, *J Solid State Chem.*, 1999, **145**, 694-704.
10 D. B. Mitzi, *Chem. Mater*., 1996, **8**, 791-800.
11 D. B. Mitzi, K. Chondroudis and C. R. Kagan, *Inorg. Chem.*, 1999, **38**, 6246-6256.
12 A. Kojima, K. Teshima, Y. Shirai and T. Miyasaka, *J. Am. Chem. Soc.*, 2009, **131**, 6050-6051.
13 M. M. Lee, J. Teuscher, T. Miyasaka, T. N. Murakami and H. J. Snaith, *Science,* 2012, **338**, 643-647.
14 M. Liu, M. B. Johnston and H. J. Snaith, *Nature*, 2013, **501**, 395-398.
15 H. Zhou, Q. Chen, G. Li, S. Luo, T. B. Song, H. S. Duan, Z. Hong, J. You, Y. Liu and Y. Yang, *Science*, 2014, **345**, 542-546.
16 W. Nie, H. Tsai, R. Asadpour, J. C. Blancon, A. J. Neukirch, G. Gupta, J. J. Crochet, M. Chhowalla, S. Tretiak, M. A. Alam, H. Wang and A. D. Mohite, *Science*, 2015, **347**, 522-525.
17 N. J. Jeon, J. H. Noh, W. S. Yang, Y. C. Kim, S. Ryu, J. Seo, S. I. Seok, *Nature*, 2015, **517**, 476-480.
18 G. E. Eperon, S. D. Stranks, C. Menelaou, M. B. Johnston, L. M. Herz, and H. J. Snaith, *Energy Environ. Sci*., 2014, **7**, 982-988.
19 G. Xing, N. Mathews, S. Sun, S. S. Lim, Y. M. Lam, M. Grätzel, S. Mhaisalkar and T. C. Sum, *Science.* 2013, **342**, 344-347.
20 Y. J. Fang, Q. F. Dong, Y. C. Shao, Y. B. Yuan and J. S. Huang, *Nat. Photonics,* 2015, DOI: 10.1038/NPHOTON.2015.156.
21 Y. Li, X. Wang, S. Wu, H. Ci, H. Xu, X. Li, H. Sun, Z. Zhang, A. Cao, X. Guo and Y. Li, *J. Mater. Chem. A,* 2015, DOI: 10.1039/c5ta04936a.
22 A. B. Wong, M. Lai, S. W. Eaton, Y. Yu, E. Lin, L. Dou, A. Fu and P. Yang, *Nano Lett.,* 2015, **15**, 5519-5524.
23 A. Fu and P. Yang, *Nat. Mater.,* 2015, **14**, 557-558.

24 Y. H. Kim, H. Cho, J. H. Heo, T. S. Kim, N. S. Myoung, C. L. Lee, S. H. Im and T. W. Lee, *Adv. Mater.*, 2015, **27**, 1248-1254.
25 L. Dou, Y. Yang, J. You, Z. Hong, W. H. Chang, G. Li and Y. Yang, *Nat. Commun.*, 2014, DOI: 10.1038/ncomms6404 .
26 H. M. Zhu, Y. P. Fu, F. Meng, X. X. Wu, Z. Z. Gong, Q. Ding, M. V. Gustafsson M.T. Trinh, Song Jin and X-Y. Zhu, *Nat Mater.*, 2015, 14, 636-643.
27 W. H. Zhang, B. Cai, *Chin. Sci. Bull.,* 2014, **59**, 2092-2101.
28 P. Gao, M. Grätzel and M. K. Nazeeruddin, *Energy Environ. Sci.*, 2014, 7, 2448-2463.
29 T. C. Sum and N. Mathews, Energy Environ. Sci., 2014, 7, 2518-2534.
30 Q. Wang, H. J. Chen, G. Liu, L. Z. Wang, *Sci. Bull.*, 2015, **60**, 405-418.
31 M. A. Green, A. Ho-Baillie and H. J. Snaith, *Nature Photon.*, 2014, **8**, 506-514.
32 M. A. Pena and J. L. G. Fierro, *Chem. Rev.*, 2001, **101**, 1981-2017.
33 C. Li, X. Lu, W. Ding, L. Feng, Y. Gao and Z. Guo, *Acta Cryst.*, 2008, 64, 702-707.
34 A. Poglitsch, D. Weber, *J. Chem. Phys.*, 1987, **87**, 6373-6378.
35 N. Kitazawa, Y. Watanabe and Y. Nakamura, *J. Mater. Sci.*, 2002, **37**, 3585-3587.
36 Y. Y. Li, C. K. Lin, G. L. Zheng, Z. Y. Cheng, H. You, W. D. Wang and J. Lin, *Chem. Mater.*, 2006, **18**, 3463-3469.
37 H. P. Xu, J. Z. Sun, A. J. Qin, J. L. Hua, Z. Li, Y. Q. Dong, H. Xu, W. Z. Yuan, Y. G. Ma, M. Wang and B. Z. Tang, *J. Phys. Chem. B*, 2006, **110**, 21701-21709.
38 W. J. Yin, T. T. Shi and Y. F. Yan, *Adv. Mater.*, 2014, **26**, 4653-4658.
39 G. E. Eperon, S. D. Stranks, C. Menelaou, M. B. Johnston, L. M. Herz and H. J. Snaith, *Energy Environ. Sci.*, 2014, **7**, 982-988.
40 T. Ishihara, J. Takahashi and T. Goto, *Solid State Commun.,* 1989, **69**, 933-936.
41 G. C. Papavassiliou and I. R. Koutselas, *Synthetic Metals,* 1995, **71**, 1713-1714.
42 C. C. Stoumpos, C. D. Malliakas and M. G. Kanatzidis, *Inorg. Chem.,* 2013, **52**, 9019-9038.
43 F. Zhang, H. Zhong, C. Chen, X. Wu, X. Hu, H. Huang, J. Han, B. Zou and Y. Dong, *ACS Nano*, 2015, **9**, 4533-4542.
44 V. D. Innocenzo, G. Grancini, M. J. P. Alcocer, A. R. S. Kandadal, S. D. Stranks, M. M. Lee, G. Lanzani, H. J. Snaith and A. Petrozza, *Nat. Commun.*, 2014, **5**, 3586-3591.
45 A. Marchioro, J. Teuscher, D. Friedrich, M. Kunst, R. van de Krol, T. Moehl, M. Grätzel and J. E. Moser, *Nat. Photonics*, 2014, **8**, 250-255.
46 V. Gonzalez-Pedro, E. J. Juarez-Perez, W. S. Arsyad, E. M. Barea, F. Fabregat-Santiago, I. Mora-Sero and J. Bisquert, *Nano Lett.*, 2014, **14**, 888-893.
47 E. J. Juarez-Perez, R. S. Sanchez, L. Badia, G. Garcia-Belmonte, Y. S. Kang, I. Mora-Sero and J. Bisquert, *Chem. Lett.*, 2014, **5**, 2390-2394.
48 M. G. Ju, G. X. Sun, Y. Zhao, W. Z. Liang, *Phys. Chem. Chem. Phys.*, 2015, **17**, 17679-17687.
49 F. Brivio, A. B. Walker and Aron Walsh, *APL Materials,* 2013, **1**, 0421111-1-5.
50 K. Yamada, T. Matsui, T. Tsuritani, T. Okuda, S. Ichiba and Z. Natur-forsch, 1990, **45a**, 307-319.
51 Q. Wang, Y. C. Shao, H. P. Xie, L. Lyu, X. L. Liu, Y. L. Gao, and J. S. Huang, *Appl. Phys. Lett.*, 2014, **105**, 163508-1-5.
52 Y. Takahashi, R. Obara, Z. -Z. Lin, Y. Takahashi, T. Naito, T. Inabe, S. Ishibashi and K. Terakura, *Dalton Trans.*, 2011, **40**, 5563-5568.
53 K. Yamada, H. Kawaguchi, T. Matsui, T. Okuda and S. Ichiba, *Bull. Chem. Soc. Jpn*, 1990, **63**, 2521-2525.
54 T. Y. Yang, G. Gregori, N. Pellet, M. Grätzel and J. Maier, *Angew. Chem.,* 2015, **127**, 8016-8021.
55 O. Knop, R. E. Wasylishen, M. A. White, T. S. Cameron and M. J. V. Oort, *Can. J. Chem.,* 1990, **68**, 412.
56 E. J. Juarez-Perez, R. S. Sanchez, L. Badia, G. Garcia-Belmonte, Y. S. Kang, I. Mora-Sero and J. Bisquert, *J. Phys. Chem. Lett.,* 2014, **5**, 2390-2394.
57 D. Weber, *Z. Naturforsch,* 1978, **33b**, 1443-1445.
58 K.N. Liang, D. B. Mitzi, and M. T. Prikas, *Chem. Mater.*, 1998, **10**, 403-411.
59 P. Qin, S. Tanaka, S. Ito, N. Tetreault, K. Manabe, H. Nishino, M. K. Nazeeruddin, M. Grätzel, *Nat. Commun.*, 2014, DOI: 10.1038/ncomms4834
60 A. Y. Mei, X. Li, L. F. Liu, Z. L. Ku, T. F. Liu, Y. G. Rong, M. Xu, M. Hu, J. Z. Chen,Y. Yang, M. Grätzel, H. W. Han, *Science*, 2014, **345**, 295-298.
61 M. R. Leyden, L. K. Ono, S. R. Raga, Y. C. Kato, S. H.Wang and Y. B. Qi, *J. Mater. Chem. A*, 2014, **2**, 18742-18745.
62 J. -H. Im, C. -R. Lee, J. -W. Lee, S. -W. Park and N. -G. Park, *Nanoscale*, 2011, **3**, 4088-4093.
63 J. H. Heo, S. H. Im, J. H. Noh, T. N. Mandal, C. -S. Lim, J. A. Chang, Y. H. Lee, H. -J. Kim, A. Sarkar, M. K. Nazeeruddin, M. Gratzel, S. I. Seok, *Nature Photon.*, 2013, **7**, 486-491.
64 S. Colella, E. Mosconi, P. Fedeli, A. Listorti, F. Gazza, F. Orlandi, P. Ferro, T. Besagni, A. Rizzo, G. Calestani, G. Gigli, F. De Angelis and R. Mosca, *Chem. Mater.*, 2013, **25**, 4613-4618.
65 N. J. Jeon, J. H. Noh, Y. C. Kim, W. S. Yang, S. Ryu, S. I. Seok, *Nature Mater.*, 2014, **13**, 897-903.
66 Z.G. Xiao, Q. F. Dong, C. Bi, Y. C. Shao, Y. B.Yuan and J. S. Huang, *Adv. Mater.*, 2014, **26**, 6503-6509.
67 J. Burschka, N. Pellet, S. J. Moon, R. Humphry-Baker, P. Gao, M. K. Nazeeruddin, Michael Grätzel, *Nature,* 2013, **499**, 316-320.
68 N. Pellet, P. Gao, G. Gregori, T.-Y. Yang, M. K. Nazeeruddin, J. Maier and M. Gratzel, *Angew. Chem. Int. Ed.*, 2014, **53**, 3151-3157.
69 Z. Song, S. C. Watthage, A. B. Phillips, B. L. Tompkins, R. J. Ellingson and M. J. Heben, *Chem. Mater.,* 2015, **27**, 4612-4619.
70 S. Colella, E. Mosconi, P. Fedeli, A. Listorti, F. Gazza, F. Orlandi, P. Ferro, T. Besagni, A. Rizzo, G. Calestani, G. Gigli, F. De Angelis and R. Mosca, *Chem. Mater.*, 2013, **25**, 4613-4618.
71 N. Yantara, F. Yanan, C. Shi, H. A. Dewi, P. P. Boix, S. G. Mhaisalkar, and N. Mathews, *Chem. Mater.*, 2015, **27**, 2309-2314.
72 Y. Tidhar, E. Edri, H. Weissman, D. Zohar, G. Hodes, D. Cahen, B. Rybtchinski and S. Kirmayer, *J. Am. Chem. Soc.,* 2014, **136**, 13249-13256.
73 S. Yang, Y. Zheng, Y. Hou, X. Chen, Y. Chen, Y. Wang, H. Zhao and H. G. Yang, *Chem. Mater.,* 2014, **26**, 6705-6710.
74 T. Kollek, D. Gruber, J. Gehring, E. Zimmermann, L. Schmidt-Mende and Sebastian Polarz, *Angew. Chem. Int. Ed.,* 2015, **54**, 1341-1346.
75 Y. C. Liu, Z. Yang, D. Cui, X. D. Ren, J. K. Sun, X. J. Liu, J. R. Zhang, Q. B. Wei, H. B. Fan, F. Y. Yu, X. Zhang, C. M. Zhao and S. Z. Liu, *Adv. Mater.,* 2015, DOI: 10.1002/adma.201502597.
76 Q. F. Dong, Y. J. Fang, Y. C. Shao, P. Mulligan, J. Qiu, L. Cao, J. S. Huang, *Science*, 2015, **347**, 967-970.
77 D. Shi, V. Adinolfi, R. Comin, M. Yuan, E. Alarousu, A. Buin, Y. Chen, S. Hoogland, A. Rothenberger, K. Katsiev, Y. Losovyj, X. Zhang, P. A. Dowben, O. F. Mohammed, E. H. Sargent and O. M. Bakr, *Science,* 2015, **347**, 519-522.
78 Q. Liao, K. Hu, H. Zhang, X. Wang, J. Yao, H. Fu, *Adv. Mater.*, 2015, DOI: 10.1002/adma.201500449.
79 M. I. Saidaminov, A. L. Abdelhady, B. Murali, E. Alarousu, V. M. Burlakov, W. Peng, I. Dursun, L. Wang, Y. He, G. Maculan, A. Goriely, T. Wu, O. F. Mohammed and O. M. Bakr, 2015, *Nat. Commun.,* DOI: 10.1038/ncomms8586.
80 S. Zhuo, J. Zhang, Y. Shi, Y, Huang and B. Zhang, *Angew. Chem. Int. Ed.,* 2015, **54**, 5693-5696.

81 E. Horváth, M. Spina, Z. Szekrényes, K. Kamarás, R. Gaal, D. Gachet and L. Forró, *Nano Lett.*, 2014, **14**, 6761-6766.
82 J. H. Im, J. Luo, M. Franckevičius, N. Pellet, P. Gao, T. Moehl, S. M. Zakeeruddin, M. K. Nazeeruddin, M. Grätzel and N. G. Park, *Nano Lett.,* 2015, **15**, 2120-2126.
83 L. C. Schmidt, A. Pertegás, S. González-Carrero, O. Malinkiewicz, S. Agouram, G. M. Espallargas, H. J. Bolink, R. E. Galian and J. Pérez-Prieto, *J. Am. Chem. Soc.,* 2014, **136**, 850-853.
84 J. -H. Im, C. -R. Lee, J. -W. Lee, S. -W. Park and N. -G. Park, *Nanoscale*, 2011, **3**, 4088-4093.
85 Y. Fu, F. Meng, M. B. Rowley, B. J. Thompson, M. J. Shearer, D. Ma, R. J. Hamers, J. C. Wright and S. Jin, *J. Am. Chem. Soc.,* 2015, **137**, 5810-5818.
86 W. M. Tian, C. Y. Zhao, J. Leng, R. R. Cui, S. Y. Jin, *J. Am. Chem. Soc.*, 2015, **137**, 12458-12461.
87 D. M. Jang, K. Park, D. H. Kim, J. Park, F. Shojaei, H. S. Kang, J. P. Ahn, J. W. Lee and J. K. Song, *Nano Lett.,* 2015, DOI: 10.1021/acs.nanolett.5b01430.
88 L. T. Dou, A. B. Wong, Y. Yu, M. L. Lai, N. Kornienko, S. W. Eaton, A. Fu, C. G. Bischak, J. Ma, T. Ding, N. S . Ginsberg, L. -W. Wang, A. P. Alivisatos, P. D. Yang, *Science*, 2015, **349**, 1518-1521.
89 P. Pistor, J. Borchert, W. Fränzel, R. Csuk, and R. Scheer, *J. Phys. Chem. Lett*., 2014, **5**, 3308-3312.
90 M. Era, T. Hattori, T. Taira and T. Tsutsui, *Chem. Mater.,* 1997, **9**, 8-10.
91 D. B. Mitzi, M. T. Prikas and K. Chondroudis, *Chem. Mater.,* 1999, **11**, 542-544.
92 Q. Chen, H. Zhou, Z. Hong, S. Luo, H. S. Duan, H. H. Wang, Y. Liu, G. Li and Y. Yang, *J. Am. Chem. Soc.,* 2014, **136**, 622-625.
93 M. Liu, M. B. Johnston and H. J. Snaith, *Nature,* 2013, **501**, 395-398.
94 J. Xing, X. Liu, Q. Zhang, S. T. Ha, Y. Yuan, C. Shen, T. C. Sum and Q. Xiong, *Nano Lett.,* 2015, DOI: 10.1021/acs.nanolett.5b01166.
95 S. T. Ha, X. Liu, Q. Zhang, D. Giovanni, T. C. Sum, Q. Xiong, *Adv. Optical Mater.,* 2014, **2**, 838-844.
96 Q. Zhang, S. T. Ha, X. Liu, T. C. Sum and Q. Xiong, *Nano Lett.,* 2014, **14**, 5995-6001.
97 H. S. Jung and N. -G. Park, *Small*, 2015, **11**, 10-25.
98 G. Hodes, *Science*, 2013, **342**, 317-318.
99 S. D. Stranks and H. J. Snaith, *Nature Nanotech*., 2015, **10**, 391-402.
100 B, O'Regan, M. Grätzel, *Nature*, 1991, **353**, 737-740.
101 A. Kojima, K. Teshima, Y. Shirai and T. Miyasaka, *J. Am. Chem. Soc.,* 2009, **131**, 6050-6051.
102 H. S. Kim,; C. R. Lee,; J. H. Im,; K. B. Lee,; T. Moehl, A. Marchioro, S. J. Moon, R. Humphry-Baker, J. -H. Yum and M. Grätzel, *Sci. Rep.,* 2012, **2**, 1-7.
103 Q. Pei, G. Yu, C. Zhang, Y. Yang, A. J. Heeger, *Science*, 1995, **269**, 1086-1088.
104 R. D. Costa, E. Ortí, H. J. Bolink, F. Monti, G. Accorsi and N. Armaroli, *Angew. Chem. Int. Ed.,* 2012, **51**, 8178-8211.
105 A. Sandström, A. Asadpoordarvish, J. Enevold and L. Edman, *Adv. Mater.,* 2014, **26**, 4974 -4974.
106 M. F. Ayguler, M. D. Weber, B. M. D. Puscher, D. D. Medina, P. Docampo, and R. D. Costa, *J. Phys. Chem. C*, 2015, **119**, 12047-12054.
107 Colin J. Humphreys, *MRS Bull*., 2008, **33**, 459-470.
108 M. H. Crawford, *IEEE J. Sel. Top. Quantum Electron*., 2009, **15**, 1028-1040.
109 D. B. Mitzi, *Prog. Inorg. Chem.,* 2007, **48**, 1-121.
110 N. K. Kumawat, A. Dey, K. L. Narasimhan and D. Kabra, *ACS Photonics*, 2015, **2**, 349-354.
111 N. K. Kumawat, A. Dey, A. Kumar, S. P. Gopinathan, K. L. Narasimhan and D. Kabra, *ACS Appl. Mater. Interfaces,* 2015, **7**, 13119-13124.
112 O. A. Jaramillo-Quintero, R. S. Sanchez, M. Rincon and I. Mora-Sero, *J. Phys. Chem. Lett.,* 2015, **6**, 1883-1890
113 G. Li, Z. K. Tan, D. Di, M. L. Lai, L. Jiang, J. H. W. Lim, R. H. Friend and N. C. Greenham, *Nano Lett.,* 2015, **15**, 2640-2644.
114 Z. K. Tan, R. S. Moghaddam, M. L. Lai, P. Docampo, R. Higler, F. Deschler, M. Price, A. Sadhanala, L. M. Pazos, D. Credgington, F. Hanusch, T. Bein, H. J. Snaith, Ri. H. Friend, *Nature Nanotech*., 2014, **9**, 687-692.
115 R. L. Z. Hoye, M. R. Chua, K. P. Musselman, G. Li, M. L. Lai, Z. K. Tan, N. C. Greenham, J. L. MacManus-Driscoll, R. H. Friend and D. Credgington, *Adv. Mater.,* 2015, **27**, 1414-1419.
116 L. Gil-Escrig, G. Longo, A. Pertegas, C. Roldan-Carmona, A. Soriano, M. Sessolo and H. J. Bolink, *Chem. Commun.,* 2015, **51**, 569-571
117 J. C. Yu, D. B. Kim, G. Baek, B. R. Lee, E. D. Jung, S. Lee, J. H. Chu, D. K. Lee, K. J. Choi, S. Cho and M. H. Song, *Adv. Mater.,* 2015, **27**, 3492-3500.
118 T. H. Maiman, *Nature,* 1960, **187**, 493-494.
119 D. A. B. Miller, *Proc. IEEE*, 2009, **97**, 1166-1185.
120 M. Groenert, C. W. Leitz, A. Pitera, V. Yang, H. Lee and R. J. Ra, *J. Appl. Phys*., 2003, **93**, 362-367.
121 B. R. Sutherland, S. Hoogland, M. M. Adachi, C. T. O. Wong and E. H. Sargent, *ACS Nano,* 2014, **8**, 10947-10952.
122 T. Kondo, T. Azuma, T. Yuasa, R. Ito, *Solid State Commun*., 1998, **105**, 253-255.
123 G. C. Xing, N. Mathews, S. S. Lim, N. Yantara, X. F. Liu, D. Sabba, M. Grätzel, S. Mhaisalkar, T. C. Sum, *Nat. Mater.,* 2014, **13**, 476-480.
124 D. B. Mitzi, *J. Mater. Chem.,* 2004, **14**, 2355-2365.
125 C. R. Kagan, T. L. Breen and L. L. Kosbar, *Appl. Phys. Lett.,* 2001, **79**, 3536-3538.
126 C. R. Kagan, D. B. Mitzi and C. D. Dimitrakopoulos, *Science*, 1999, **286**, 945-947.
127 D. B. Mitzi, C. D. Dimitrakopoulos and L. L. Kosbar, *Chem. Mater.*, 2001, **13**, 3728-3740.
128 D. B. Mitzi, C. D. Dimitrakopoulos, J. Rosner, D. R. Medeiros, Z. Xu and C. Noyan. *Adv. Mater.*, 2002, **14**, 1772-1776.
129 X. Y. Chin, D. Cortecchia, J. Yin, A. Bruno and C. Soci, *Nat. Commun.,* 2015, DOI: 10.1038/ncomms8383.
130 H. H. Fang, R. Raissa, M. Abdu-Aguye, S. Adjokatse, G. R. Blake, J. Even and M. A. Loi, *Adv. Funct. Mater*., 2015, **25**, 2378-2385.
131 J. J. Wang, F. F. Cao, L. Jiang, Y. G. Guo, W. P. Hu and L. J. Wan, *J. Am. Chem. Soc*., 2009, **131**, 15602-15603.
132 H. Kind, H. Yan, B. Messer, M. Law and P. Yang, *Adv. Mater.,* 2002, **14**, 158-160.
133 H. R. Xia, J. Li, W. T. Sun and L. M. Peng, *Chem. Commun.,* 2014, **50**, 13695-13697.
134 Y. Takahashi, H. Hasegawa, Y. Takahashi and T. Inabe, *J. Solid State Chem.,* 2013, **205**, 39-43.
135 Y. Guo, C. Liu, H. Tanaka and E. Nakamura, *J. Phys. Chem. Lett.,* 2015, **6**, 535-539.
136 X. Hu, X. Zhang, L. Liang, J. Bao, S. Li, W. Yang and Y. Xie, *Adv. Funct. Mater.,* 2014, **24**, 7373-7380.
137 H. W. Chen, N. Sakai, A. K. Jena, Y. Sanehira, M. Ikegami, K. C. Ho and T. Miyasaka, *J. Phys. Chem. Lett.,* 2015, **6**, 1773-1779.
138 D. Li, G. Dong, W. Li and L. Wang, *Sci. Rep.,* 2014, DOI: 10.1038/srep07902
139 C. Liu, K. Wang, C. Yi, X. Shi, P. Du, A. W. Smith, A. Karim and X. Gong, *J. Mater. Chem. C,* 2015, **3**, 6600-6606.
140 B. R. Sutherland, A. K. Johnston, A. H. Ip, J. Xu, V. Adinolfi, P. Kanjanaboos and E. H. Sargent, *ACS Photonics,* **2015**, *2* , 1117-1123.
141 R. Dong, Y. Fang, J. Chae, J. Dai, Z. Xiao, Q. Dong, Y. Yuan, A. Centrone, X. C. Zeng and J. Huang, *Adv. Mater.,* 2015, **27**, 1912-1918.
142 Y. J. Fang and J. S. Huang, *Adv. Mater.,* 2015, **27**, 2804-2810.

143 H. Deng, D. Dong, K. Qiao, L. Bu, B. Li, D. Yang, H.E. Wang, Y. Cheng, Z. Zhao, J. Tang and H. Song, *Nanoscale*, 2015, **7**, 4163-4170.
144 M. He, Y. Chen, H. Liu, J. Wang, X. Fang and Z. Liang, *Chem. Commun.,* 2015, **51**, 9659-9661.
145 Y. Lee, J. Kwon, E. Hwang, C. H. Ra, W. J. Yoo, J. H. Ahn, J. H. Park and J. H. Cho, *Adv. Mater.,* 2015, **27**, 41-46.
146 M. Spina, M. Lehmann, B. Náfrádi, L. Bernard, E. Bonvin, R. Gaál, A. Magrez, L. Forró and E. Horváth, *Small,* 2015, DOI: 10.1002/smll.201501257.